The Astrophysical Journal, 602:181–189, 2004 February 10

INTEGRAL FIELD SPECTROSCOPY OF THE EXTENDED IONIZED GAS IN ARP 220[1]

Luis Colina,[2] Santiago Arribas,[3,4] and David Clements[5]

Received 2003 July 28; accepted 2003 October 17

ABSTRACT

Integral field optical spectroscopy with the INTEGRAL system has been used to investigate for the first time the two-dimensional kinematic and ionization properties of the extended, warm, ionized gas in Arp 220 over an area of $75\farcs0 \times 40\farcs0$ (i.e., 28×15 kpc). The structure of the ionized gas is divided into well-identified regions associated with the X-ray–emitting plumes and extended lobes, previously studied in detail by McDowell and collaborators. The overall ionization state of the warm gas in the plumes and lobes, as traced by the [N II]/Hα line, is consistent with high-velocity shocks expanding in a neutral ambient medium. Changes in the ionization state of the gas along the major axis of the plumes are detected, in particular in the outer regions of the northwestern plume, where the transition between the main stellar body of the galaxy and a broad, low surface brightness tidal tail is located. If the plumes are produced by a starburst-driven galactic wind, the efficiency in the conversion of mechanical to radiation energy is a factor of at least 10 smaller than in galactic winds developed in edge-on spiral galaxies with well-defined rotation and axis of outflow. The kinematic properties of the lobes, with an average velocity of +8 km s^{-1} (east lobe) and -79 km s^{-1} (west lobe), are to a first order in agreement with the predictions of the merger scenario, according to which the lobes are tidally induced gas condensations produced during the merging process. The largest velocity gradients of 50 km s^{-1} kpc^{-1} and velocity deviations of up to +280 and -320 km s^{-1} from the systemic velocity are associated not with the plumes but with the outer stellar envelope and broad tidal tails at distances of up to 7.5 kpc, indicating that the large-scale kinematics of the extended ionized gas in Arp 220 is most likely dominated by the tidally induced motions, and not by galactic winds associated with nuclear starbursts.

Subject headings: galaxies: active — galaxies: individual (Arp 220) — galaxies: interactions — galaxies: nuclei — galaxies: starburst

On-line material: color figures

1. INTRODUCTION

Arp 220 is the prototypical cool (i.e., $f_{25}/f_{60} < 0.2$) ultraluminous infrared galaxy (ULIRG), with an infrared luminosity $L_{\rm IR}(8\text{–}1000\ \mu{\rm m}) = 1.45 \times 10^{12}\ L_\odot$. Arp 220 is also the nearest ULIRG, with a redshift of 0.01813, and is thus an ideal laboratory to investigate the physical processes taking place in ULIRGs.

Arp 220 has clear signs of being at the final stage of a merging process. Optical images reveal extended, broad tidal tails (Arp 1966; Hibbard, Vacca, & Yun 2000; Surace, Sanders, & Evans 2000), and high-resolution near-infrared (NIR) and radio imaging show the presence of two nuclei separated by about 0.4 kpc (i.e., $0\farcs98$; Carico et al. 1990; Graham et al. 1990; Baan & Haschick 1995; Scoville et al. 1998, 2000 and references therein). Moreover, Arp 220 is also extraordinarily rich in gas, with about $5 \times 10^9\ M_\odot$ of molecular gas ($M_{\rm H_2}$) concentrated in the nuclear region of 250 pc in radius (Scoville, Yun, & Bryant 1997).

The stellar and the cold gas components have been studied in detail (Scoville et al. 1997; Sakamoto et al. 1999; Hibbard et al. 2000; Surace et al. 2000 and references therein). The two NIR/molecular nuclei and their associated disks—which rotate in opposite directions—are embedded in a kiloparsec-scale molecular disk and seem to rotate in the same sense as the 100 kpc scale H I disk, suggesting a prograde-retrograde encounter of two gas-rich spiral galaxies (Scoville et al. 1997).

The ionized gas component in the nuclear regions of Arp 220 has been studied on the basis of long-slit observations along two position angles (Heckman, Armus, & Miley 1990) and, more recently, using integral field spectroscopy with INTEGRAL (Arribas, Colina, & Clements 2001, hereafter ACC01). The detailed two-dimensional study by ACC01 has shown the complex kinematical behavior of the ionized gas within 2 kpc of the dust-enshrouded nucleus, where three different components associated with rotation and radial flows have been identified.

The nuclear and extended X-ray–emitting gas has also been investigated with *ROSAT* PSPC images (Heckman et al. 1996) and, more recently, with *Chandra* high spatial resolution X-ray imaging (Clements et al. 2002; McDowell et al. 2003, hereafter McD03). The *Chandra* images show the presence of four distinct, spatially separated emitting regions, the hard X-ray nucleus, the circumnuclear region, the extranuclear plumes, and the extended lobes, that could be associated with different phenomena operating at different physical scales, i.e., the dust-enshrouded AGN (nucleus), the (circum-)nuclear starburst and associated winds (circumnuclear regions and plumes,

[1] Based on observations with the William Herschel Telescope (WHT), operated on the island of La Palma by the Isaac Newton Group (ING) in the Spanish Observatorio del Roque de los Muchachos of the Instituto de Astrofísica de Canarias.

[2] Instituto de Estructura de la Materia, Consejo Superior de Investigaciones Científicas (CSIC), Serrano 121, 28006 Madrid, Spain; colina@isis.iem.csic.es.

[3] Space Telescope Institute, 3700 San Martin Drive, Baltimore, MD 21218; arribas@stsci.edu. Also affiliated with the Astrophysics Division, Space Science Department of the European Space Agency.

[4] On leave from the Instituto de Astrofísica de Canarias–CSIC.

[5] Physics Department, Imperial College, Prince Consort Road, London SW7 2BW, UK; d.clements@ic.ac.uk.

respectively), and the tidal forces produced during the interaction (extended lobes).

However, a detailed kinematical and ionization study of the gas flows present in the extended ionized gas of Arp 220 and how they are affected by the interaction process and the massive nuclear starburst is still lacking and requires an observational technique able to obtain two-dimensional velocity fields and ionization maps of the complex ionized gas structures detected in this galaxy over scales of about 60″ across. Integral field spectroscopy (IFS; e.g., Arribas & Mediavilla 2000) is an ideal technique for such a study, since it allows a simultaneous and complete mapping of both the kinematic and ionization properties of the warm ionized gas over large areas (see Arribas & Colina 2003 and references therein for previous studies of ULIRGs using integral field spectroscopy).

This paper presents the first two-dimensional spectroscopic study of the extended ionized nebula in Arp 220 covering a region of 75″ × 40″. In the following sections, the stellar morphology (§ 3.1), two-dimensional structure (§ 3.2), ionization (§ 3.3), and kinematics (§ 3.4) of the ionized gas are presented. The origin of the extended ionized gas, as produced by starburst-driven galactic winds (§ 4.1) and tidal forces during the merger process (§ 4.2), are briefly discussed. Throughout the paper, a distance of 77.6 Mpc is assumed. At the assumed distance, 1″ corresponds to 375 pc.

2. OBSERVATIONS AND DATA REDUCTION

Integral field spectroscopy of Arp 220 was obtained with the INTEGRAL system (Arribas et al. 1998) and the WYFFOS spectrograph (Bingham et al. 1994) in the 4.2 m William Herschel Telescope. We used the wide-field observing mode (i.e., bundle of fibers SB3), which consists of 115 fibers, each 2.″7 in diameter, covering a 33.″6 × 29.″4 field of view. In addition, 20 fibers, distributed in a circle 45″ in radius, were used for simultaneous sky measurements. The spectra were taken using a 600 lines mm^{-1} grating with an effective resolution of about 9.8 Å and covering the 4500–7500 Å spectral range. The observations consisted of a mosaic of three pointings (nucleus, east nebula, and west nebula), covering almost completely a rectangular area of 75″ × 40″ (see Fig. 1). The total integration time in each of the pointings, split into separate integrations of 1500 s each, was 6000 s for the nucleus, 15,000 s for the east nebula, and 18,000 s for the west nebula. The seeing (1.″1–1.″2) was very stable over the entire observing period (two nights), and conditions were spectrophotometric.

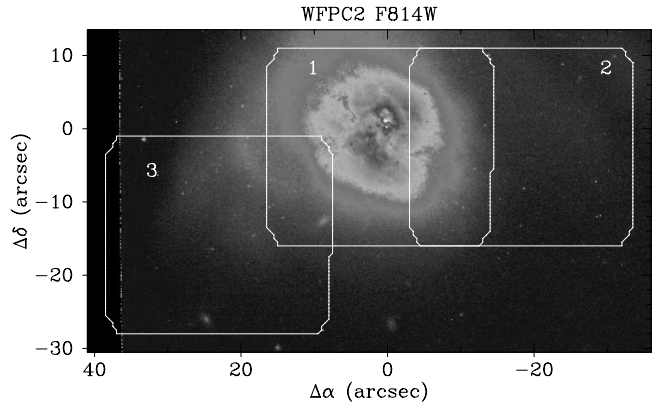

FIG. 1.—Archival WFPC2 *I*-band image of Arp 220 showing the central regions, as well as the extended, low surface brightness envelope. The overlays indicate the area covered by the three independent pointings with INTEGRAL. North is up, and east is left. [*See the electronic edition of the Journal for a color version of this figure.*]

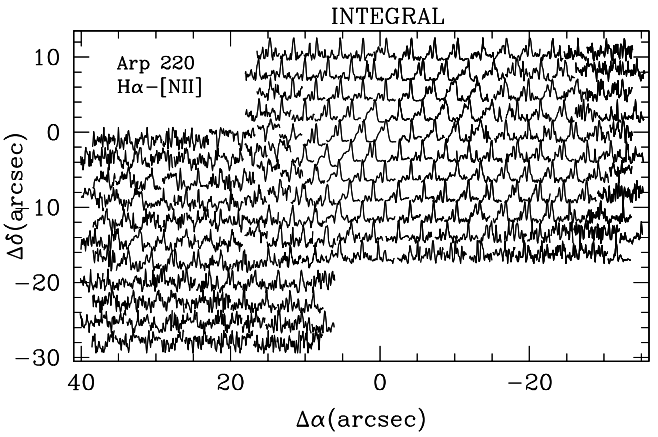

FIG. 2.—Spatial distribution of the spectra around the redshifted Hα+[N II] spectral region obtained after the data reduction process is completed, including internal cross-calibration of the three pointings using the spectra on the overlapping regions.

Data reduction followed the standard procedures applied to spectra obtained with two-dimensional fiber spectrographs, which have been explained elsewhere (Arribas et al. 1997 and references therein; see also ACC01). The two-dimensional distribution of the reduced spectra in the range of the redshifted Hα and [N II] lines is presented in Figure 2. The changes in the profiles of the lines and in the ionization conditions (i.e., [N II]/Hα ratio) are obvious even from this figure alone.

The absolute calibration was obtained observing the standard star SP 1550+330 with the same system configuration and data reduction procedures as used for Arp 220. The relative calibration of the different pointings agrees to within 20%, as obtained by comparing the regions of overlapping. Taking into account additional uncertainties, such as the reliability of the Hα and [N II] line fits, the uncertainty in the absolute calibration is about 30%.

3. RESULTS

3.1. *Stellar Structure*

The reduced two-dimensional spectra can be used to generate continuum and emission-line images by selecting specific wavelength windows. A red, narrowband (7425–7455 Å) continuum image (Fig. 3) is generated for a direct comparison with the archival *Hubble Space Telescope* (*HST*) WFPC2 *I*-band (F814W filter; PI K. Borne) image of Arp 220 (Fig. 1). The INTEGRAL red continuum image shows an overall stellar morphology in the nuclear regions similar to the structure detected in the WFPC2 *I*-band image, although with a poorer spatial resolution. In particular, the nuclear dust lane that cuts the stellar distribution in half is clearly visible, with the apparent optical nucleus, identified as the continuum peak at these wavelengths, located northwest of it. The position of this peak, which corresponds to α(B1950.0) = $15^h32^m46^s.8$ and δ(B1950.0) = 23°41′09.″3, with an uncertainty of 1.″0, is offset from the infrared and radio nucleus by 1.″5–2.″0 (see ACC01).

An additional feature worth mentioning is the disrupted stellar light distribution in the outer regions at distances between 4 and 11 kpc, i.e., 10.″0–30.″0, from the nucleus (see Fig. 3). These regions correspond most likely to tidal tails and

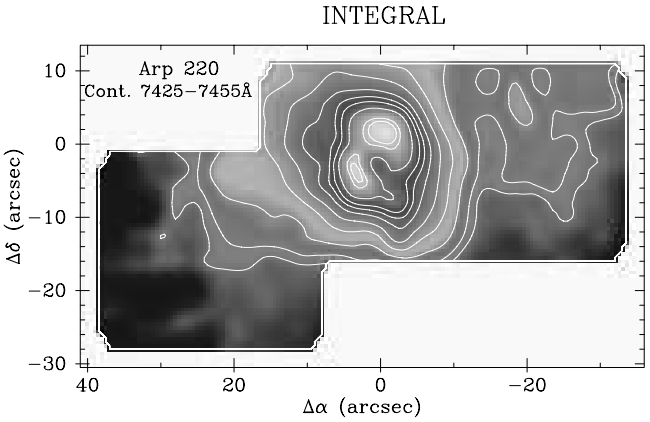

FIG. 3.—INTEGRAL image of the stellar light distribution in the central regions and faint extended envelope of Arp 220, as traced by a line-free red narrowband continuum window (7425–7455 Å) generated using all SB3 spectra. Note that the overall structure is similar to that detected in the higher resolution *HST* image (Fig. 1), although with a poorer resolution. The contours are in arbitrary units and represent 5%, 7%, 12%, 18%, 26%, 36%, 45%, 53%, 72%, and 92% of the innermost contour. As in Fig. 1, north is up, and east is to the left. [*See the electronic edition of the Journal for a color version of this figure.*]

external regions of the stellar disks in the progenitor galaxies involved in the merger. The faint northwestern tail detected in the WFPC2 image (Fig. 1) is clearly identified in the low-resolution INTEGRAL continuum image (Fig. 3) as a broad structure centered at about 20″.0 (i.e., 7.5 kpc) northwest of the nucleus and elongated almost parallel to the dust lane orientation for about 7 kpc. On the eastern side, the stellar envelope extends toward the southeast up to a distance of about 30″.0 (i.e., 11 kpc). While the major axis of the nuclear stellar light distribution is given by the central dust lane along position angle (P.A.) $45^\circ \pm 5^\circ$, the extended stellar envelope, as seen also in the WFPC2 image and in previous deep, ground-based images (Hibbard et al. 2000), has a major axis oriented along P.A. 110°, away from that of the dust lane and almost perpendicular to it. All these characteristics point to a stellar system in Arp 220 that, as a consequence of the merging process, has not yet reached its dynamically relaxed configuration.

3.2. *Extended Ionized Gas: Structure*

The major axis of the diffuse, optical ionized gas in Arp 220 has an end-to-end size of 24 kpc, similar in length to the extended soft X-ray–emitting regions (Heckman et al. 1996; McD03). The ionized gas distribution traced by the Hα (Fig. 4*a*) and [N II] 6584 Å (Fig. 4*b*) emission lines clearly shows substructures and different components at various linear scales. As originally noted by Heckman et al. (1996) and recently confirmed with higher spatial resolution *Chandra* images (McD03), the structure of the extended X-ray emission bears a strong morphological resemblance to the warm, ionized gas traced by the optical emission lines. For consistency with the different components of the X-ray–emitting gas already identified, we also refer in the rest of the paper to the circumnuclear regions, plumes, and lobes, to identify the optical ionized gas regions at various scales. A summary of several observed and derived properties for the different regions is given in Table 1.

3.2.1. *The Nucleus and Circumnuclear Region*

The nucleus and its surrounding circumnuclear region, up to a radius of 2 kpc, have already been investigated in more detail using INTEGRAL with a higher spatial and spectral resolution configuration (see ACC01 for details). The Hα emission peaks at 0″.8 (i.e., 0.3 kpc) southwest of the optical stellar continuum peak and coincides with the position of the soft X-ray emission peak, which is displaced 1″.5 northwest of the hard X-ray emission source (Clements et al. 2002). The hard X-ray source agrees in position with the mid-infrared and brightest radio sources (Soifer et al. 2000), and it is consequently considered the true nucleus of Arp 220. Therefore, the warm, Hα ionized gas associated with the nuclear hard X-ray source is enshrouded by the nuclear dust lane and appears distributed with an apparent emission peak displaced 0.6 kpc northwest of the true ionizing nucleus.

3.2.2. *The Plumes*

On a scale of a few kiloparsecs and up to distances of 4 kpc from the nucleus, two elongated, high surface brightness regions, one on each side of the nucleus, with a total length of 7 kpc, are identified. These regions, oriented along a P.A. of

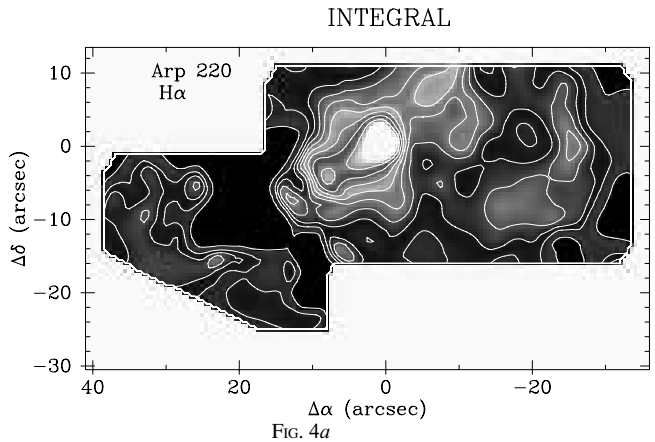

FIG. 4*a*

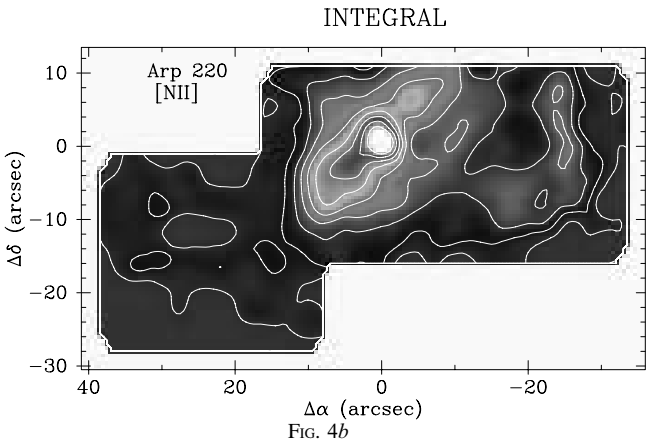

FIG. 4*b*

FIG. 4.—INTEGRAL images of the ionized gas distribution, as traced by the (*a*) Hα and (*b*) [N II] 6583 Å lines. The three different regions identified in X-rays, the bright circumnuclear region, the elongated plumes, and the extended, diffuse lobes, are easily identified here. Changes in the ionization structure of the plumes, traced by the offsets between the Hα and [N II] emission peaks, are clearly visible. The contours for Hα represent surface brightness levels of 0.1%, 0.8%, 1.9%, 3.8%, 6.9%, 12.1%, 20.8%, 35.4%, 59.6%, and 100% of the maximum level (6.8×10^{-16} ergs cm^{-2} s^{-1} arcsec^{-2}). The orientation is the same as in previous figures. [*See the electronic edition of the Journal for a color version of this figure.*]

TABLE 1

PROPERTIES OF THE EXTENDED IONIZED REGIONS IN ARP 220

Region[a]	Distance[b] (kpc)	P.A.[a]	Extent (kpc)	$F_{obs}(H\alpha)$[c]	$\log L(H\alpha)$[d] (ergs s^{-1})	$M_{H\alpha}$[e] ($10^4\ M_\odot$)	$V_{average}$[f] (km s^{-1})	E_k[g] (10^{49} ergs)
Circumnuclear	0	...	1.1 × 1.1	31.0	40.4	84.6	5397 ± 74	...
NW plume Hα	3.5	320	1.5 × 1.9	1.9	39.1	4.4	5305 ± 39	4
NW plume [N II]	2.6	320	1.3 × 1.3	1.0	38.8	2.4	5291 ± 21	3
SE plume Hα	3.5	125	2.4 × 2.4	5.4	39.6	14.6	5404 ± 58	...
SE plume [N II]	2.0	125	2.3 × 2.3	4.5	39.5	12.3	5389 ± 61	...
W lobe	7.0	260	7.1 × 7.5	9.3	39.8	21.5	5321 ± 54	14
E lobe	10.1	114	8.3 × 5.6	2.1	39.2	5.4	5408 ± 76	...

[a] Regions labeled "NW plume Hα" and "NW plume [N II]" are the regions identified in the NW plume with the Hα and [N II] emission peaks, respectively. The same applies for regions SE plume Hα and SE plume [N II].

[b] For the plumes, the distance between the nucleus and the local Hα and [N II] peak emission in the plumes; for the lobes, the distance between the nucleus and the midpoint of the structure traced by the [N II] emission. The nucleus is identified here as the central bright source, even if this does not correspond with the true dust-enshrouded nucleus of the galaxy, not visible in the optical.

[c] Flux in units of 10^{-15} ergs s^{-1} cm^{-2} A^{-1}; uncertainties of 10%–15%.

[d] Luminosity not corrected by internal extinction.

[e] Mass of ionized gas, assuming an average density of 100 cm^{-3}.

[f] The systemic velocity is 5400 ± 20 km s^{-1}, from previous INTEGRAL measurements (ACC01). Velocities as measured and not corrected for projection effects.

[g] Kinetic energy, assuming the mass and average velocity given in previous two columns and a systemic velocity of 5400 km s^{-1}.

120°–320°, coincide with the X-ray–emitting northwest and southeast plumes (hereafter NW and SE plumes; McD03). As for the soft X-ray emission, the surface brightness of the outer part of the SE plume, not affected by the absorption due to the central dust lane, is a factor of 4 that of the NW plume (Fig. 4), indicating a clear, intrinsic asymmetry in the properties of the warm and hot ionized gas in opposite directions of the dust-enshrouded nucleus. The close similarity of the [N II]+Hα and the X-ray plumes in relative surface brightness (i.e., the SE plume is brighter than the NW plume by the same factor in both Hα and X-ray emission) and morphology (see Fig. 9 in McD03) indicates that the warm and hot ionized gas components are closely related and most likely have the same physical origin (see § 4 for further discussion).

As mentioned above, the line-emitting gas in the SE plume has on average a surface brightness 4 times that of the NW plume. There are several mechanisms that can be invoked to explain this asymmetry, but none of them is clearly supported by the present set of data. Assuming the same geometry for both plumes and that they are viewing the same radiation field coming from the nucleus, this enhancement in brightness could be explained by a density effect. Since Hα and [N II] emission are a function of N_e^2, a difference of 4 in surface brightness would imply a difference of 2 in density, and therefore the gas in the SE plume would be a factor of 2 more dense than the corresponding gas in the NW plume. However, there is no clear evidence for this systematic difference in the electron density of the ionized gas. The measured [S II] 6717–6731 Å emission-line ratio gives values of the order of 1.0–1.1, consistent with an average density of a few hundred particles per unit of volume in both the SE and NW plumes. An alternative explanation could be that the NW plume is seen through the dust lane, the intrinsic emission more absorbed, and consequently the surface brightness diminished, relative to that of the SE plume. Although the nondetection of the Hβ line in emission precludes any quantitative estimate of the local extinction using the Balmer decrement, this scenario also seems not to be valid, since there is no evidence for a radial dependency of the NW and SE plumes' relative surface brightness. In addition, a factor of 4 in absorption would imply an almost constant extinction equivalent to 3 mag in the visual over distances of several kiloparsecs, which seems very unlikely in view of the nonuniform structure of the dust lane, which also runs almost perpendicular to the orientation of the plumes. A likely explanation for the difference in surface brightness is that the radiation field seen by the gas in the plumes, i.e., at distances of few to several kiloparsecs, is not symmetric with respect to the nucleus. This could be the case if the three-dimensional structure of the dense dust and gas in the nuclear regions surrounding the dust-enshrouded nucleus were such that it would block the radiation preferentially along a given direction.

At a lower surface brightness, there is a secondary plume (or filament), located south of the NW plume and elongated mostly parallel to it from (−5.″0, −4.″0) to (−12.″0, +8.″0), with a total length of about 10.″0 (i.e., 3.75 kpc). The southwestern part of this secondary plume, brightest in [N II] light, emerges from the main circumnuclear emission peak (see Fig. 4*b*), while the northwestern part of it, traced by the Hα line, curves at (−10.″0, +1.″0) to reconnect with the NW plume at its tip (see Fig. 4*a*).

3.2.3. *The Lobes*

On scales of several kiloparsecs, at distances between 4 and 15 kpc from the nucleus, the Hα and [N II] light distributions show the presence of two extended, limb-brightened lobes, one on each side of the nucleus. The west lobe (hereafter W lobe) is about a factor of 3 brighter than the east lobe (hereafter E lobe) and has an edge-brightened structure, with a diameter of about 4.5 kpc, centered at 7 kpc west of the nucleus. On the other hand, the low surface brightness E lobe, centered at 9.4 kpc from the nucleus, is actually located southeast of the nucleus and has an ellipsoidal, edge-brightened shape, with a major axis of about 9 kpc oriented along a P.A. of 90° (Fig. 4*b*).

An additional important feature is that the ionized gas in the lobes tends to avoid the regions occupied by the extended stellar envelope in the southeast and by the broad tidal tails detected in the northwest (see Figs. 3 and 4*b*). Moreover, the optical lobes also avoid the neutral H I gas distribution that is located at about the same radial distances from the nucleus but at a P.A. of 50° (Hibbard et al. 2000). On the contrary, as already known from previous studies (Heckman et al. 1996;

McD03), the overall structure of the optical lobes coincides with that of the X-ray lobes. This spatial segregation between, on one side, the warm and hot gas and, on the other side, the stellar and the cold neutral gas could favor the idea that the observed stellar and gas distributions in the outer regions of a merger system like Arp 220 are the result of the tidal forces induced during the merging process. Therefore, the structure and energetics of the ionized gas in these lobes are not associated with a starburst-generated wind but with the tidal forces and evolutionary state of the merger (see § 4.2 and McD03 for further discussions).

3.3. *Extended Ionized Gas: The Ionization State*

3.3.1. *The Nucleus and Circumnuclear Region*

The ionization state of the circumnuclear region has been studied in more detail in ACC01. However, the main results are briefly summarized here in order to get a complete picture of the ionization of the gas at different scales. Because of the absorption caused by the dust lane, the nucleus itself, identified as the hard X-ray, infrared, and radio emission peak, is not detected as the brightest region in emission lines. As mentioned in § 3.2.1, the peak of the Hα and [N II] emission-line distributions is located at about 1.″5 northwest (0.6 kpc) of the dust-enshrouded nucleus. The ionization structure of the warm gas in the circumnuclear regions is very homogeneous, with a few well-localized regions where a change in the ionization state is detected (ACC01). On average, the overall ionization is consistent with LINER-like emission, or even a Seyfert 2–like nebula around the peak ionized gas emission, if the lower limits to the [O III]/Hβ and [O I]/Hα ratios are considered (see ACC01 for further details).

3.3.2. *The Plumes*

The ionization state of the plumes presents a complex structure, with well-identified regions along their major axes where the excitation conditions change on the scale of kiloparsecs. The circumnuclear Hα and [N II] main emission peaks located northwest of the dust-enshrouded nucleus are spatially coincident. However, the Hα and [N II] secondary emission peaks are offset by about 1–1.4 kpc and present a clear pattern. The [N II] secondary peaks in the SE and NW plumes are located at distances of about 2 and 2.6 kpc from the main emission peak, respectively. On the other hand, the Hα secondary peaks are located at the tips of the plumes, at distances of about 3.5 kpc. The average ionization state of the gas in the plumes is characterized by an [N II]/Hα ratio of the order of 1.4–2.0, presenting a maximum value of 3 in the region identified as the [N II] emission peak in the NW plume. Similarly, the [S II]/Hα ratios have values of about 1, with a slightly larger value in the region of the [N II] emission peak. Values this large for the [N II] and [S II] emission lines with respect to Hα are consistent with high-velocity shocks ($\sim$300 km s^{-1}) expanding in a neutral, not preionized, medium (Dopita & Sutherland 1995).

The ionization state in the secondary plume/filament south of the NW plume (see § 3.2.2 for details on its orientation and length) also presents very interesting features. Ionization gradients are clearly visible in this plume, as traced by the regions of Hα and [N II] high surface brightness. While the southwestern region of the secondary plume, emerging from the main line-emitting peak, emits mostly in [N II] light, the Hα emission takes over in the curved northwestern region that reconnects this secondary plume with the tip of the NW plume (see Fig. 4). The change in the ionization, in particular the enhancement of Hα with respect to [N II], appears in a region where an abrupt change in the velocity of the gas by about 50–60 km s^{-1} kpc^{-1} is detected (see § 3.4.2 and Figs. 5*a* and 5*b*).

3.3.3. *The Lobes*

The ionized gas in the extended lobes is asymmetrically distributed, with the W lobe being on average a factor of 4 brighter than the E lobe. The ionization state, as traced by the [N II]/Hα ratio (1.10–1.4), is very uniform over the entire extension of the lobes, without any indication of ionization gradients or substructures at the present resolution (3″, or about 1.1 kpc). As for the plumes, the detection of strong [N II] emission with respect to Hα ([N II]/Hα ratio between 1.1 and 1.4) is consistent with high-velocity shocks evolving in a neutral, not preionized, medium, although additional measurements of the [O III]/Hβ ratio would be needed to confirm this (see Dopita & Sutherland 1995). The average density of the ionized gas in the W lobe is lower than that in the plumes and less than 100 electrons cm^{-3}, as measured by the [S II] line ratio. The weakness of the [S II] line emission in the SE lobe precludes any measurement of the density in this region.

3.4. *Extended Ionized Gas: Velocity Field*

The large-scale velocity field over the entire region of about 75.″0 × 40.″0 has been traced by the [N II] 6584 Å emission line (see Fig. 5). The velocity field is rather complex, without any regular pattern but with substructures and large velocity gradients already visible on scales of 1–1.5 kpc that can be associated with different structures identified in the stellar and gas components. The systemic velocity (*cz*) of Arp 220, defined as the velocity of the gas located in the region of the dust-enshrouded nucleus, is 5400 $\pm$ 20 km s^{-1} (ACC01). The velocities mentioned in the following sections are given relative to this value.

3.4.1. *The Nucleus and Circumnuclear Region*

The velocity field in this region shows a very complex behavior, characterized by the presence of at least three kinematically and spatially separated components associated with rotation and radial flows. A detailed investigation of the gas motions in these regions can be found in ACC01.

3.4.2. *The Plumes*

The velocity field of the SE and NW plumes show a very different structure. The NW plume shows a smooth velocity field with an average approaching velocity of -102 ± 37 km s^{-1} and a very small velocity gradient of less than 5 km s^{-1} kpc^{-1}. On the contrary, the SE plume has an average velocity of -4 ± 63 km s^{-1}, i.e., consistent with the systemic velocity, but it presents large velocity gradients. In particular, while the inner parts of the SE plume, i.e., those closer to the dust-enshrouded nucleus, show a velocity similar to the systemic one, the outer regions, identified by the tip of the [N II] emission and by the local Hα emission peak, show velocity changes from about systemic, or even approaching, velocity up to +100–120 km s^{-1}, implying velocity gradients of about 70–100 km s^{-1} kpc^{-1}.

The velocity structure of the secondary plume/filament is such that the gas is moving with a velocity of -25 km s^{-1} in the southwestern region connecting with the [N II] and Hα main emission peak, which increases to +85 km s^{-1} at 10.″0 northwest of the emission peak and decreases again to about -50 km s^{-1} in the region where this filament reconnects with

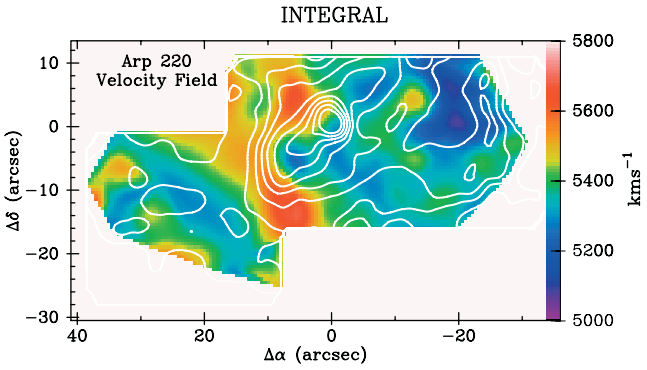

FIG. 5*a*

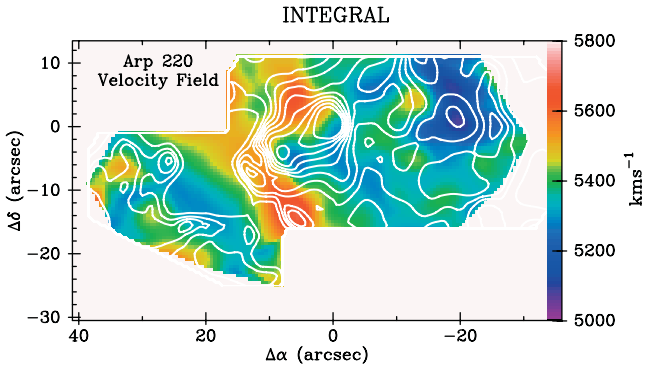

FIG. 5*b*

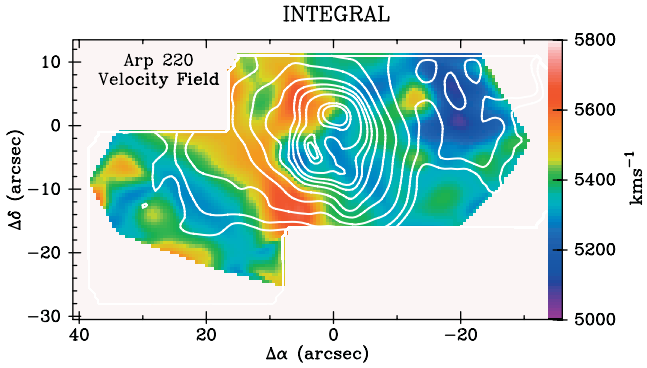

FIG. 5*c*

FIG. 5.—Velocity field of the extended ionized gas obtained from the [N II] 6583 Å emission line. The superposed contours in (*a*), (*b*), and (*c*) represent the [N II], Hα, and stellar light distribution, respectively.

the tip of the NW plume, where an approaching velocity of -115 km s^{-1} has been measured.

It is difficult to explain the very different kinematical behavior observed in the plumes under the simple scenario of a symmetric biconical outflow having a common origin in the dust-enshrouded nucleus. Differences in the physical conditions and/or kinematics of the interstellar medium, interactions between several gas systems moving with large relative velocities, and/or different relative orientations of the axes of outflow in the plumes have to be invoked before reaching any conclusion about the origin and evolution of the plumes (see discussion in § 4).

3.4.3. *The Lobes*

The velocity field of the ionized gas in the lobes indicates that the W lobe is approaching with an average velocity of -79 ± 58 km s^{-1}, while the E lobe has a velocity of $+8 \pm 79$ km s^{-1}, consistent with the velocity of the system. Therefore, the average velocity of the lobes is consistent, although with a larger dispersion, with that of their corresponding plumes, independent of the overall physical scale of the two structures and the different orientations of their major axis. The W lobe has a velocity field with a maximum receding velocity of +30 km s^{-1} and a minimum approaching velocity of about -160 km s^{-1} at 25″.0 (i.e., 9.4 kpc) east of the nucleus. The southern section of this lobe has approaching velocities of up to -70 km s^{-1}. The ionized gas in the E lobe also has approaching velocities in the -25 to -60 km s^{-1} range, with a maximum velocity of only +10 km s^{-1}, consistent with the systemic velocity.

Another important aspect of the ionized gas located in the limb-brightened lobes is its different kinematical behavior with respect to the corresponding gas associated, at least in projection, with the southeastern stellar envelope and the broad, northwestern tidal tail. This velocity difference amounts to +75 and +190 km s^{-1} for the gas in the E and W lobes, respectively (see § 3.4.4). These large velocity differences suggest that the relatively high surface brightness lobes are physically separated and kinematically distinct from the low surface brightness, merger-induced stellar envelope and tidal tail (see § 4.2 for a more detailed discussion).

3.4.4. *Diffuse Gas Associated with the Stellar Envelope and Tidal Tail*

In addition to the ionized gas associated with the X-ray–emitting plumes and lobes, there are low surface brightness ionized gas regions that seem to be associated with stellar structures that have been produced by the tidal forces generated during the evolution of the merger. These regions are identified as the extended stellar envelope southeast of the nucleus and the broad, low surface brightness tidal tail northwest of the nucleus.

Although the ionized gas in these regions represents a minor contribution to the overall content, both in mass and energy, the largest deviations from systemic velocity are detected in these low surface brightness regions, and the velocity substructure of this diffuse gas follows precisely the changes detected in the structure of the stellar light distribution (see Fig. 5*c*). The gas in the southwestern side of the central dust lane moves with velocities of -110 km s^{-1}. Moreover, the gas associated with the broad stellar tidal tail located at about 20″.0 west of the

nucleus is moving with an approaching velocity of up to -320 km s^{-1}, representing the absolute minimum of the overall velocity field. On the other hand, low surface brightness gas associated with the southeastern stellar envelope shows velocities ranging from -100 to $+100$ km s^{-1}, with a maximum value of $+280$ km s^{-1} at about 7.″0 northeast and 17.″0 southeast of the nucleus, representing the absolute maximum of the entire velocity field. In summary, the gas in these regions presents the largest velocity deviations measured in the extended ionized regions of Arp 220, with a peak-to-peak value of 600 km s^{-1} at distances of about 5–7.5 kpc from the nucleus.

4. DISCUSSION

4.1. *Origin of the Plumes: Starburst-driven Galactic Wind Structures?*

Starburst-driven galactic winds, understood as generated by the collective effects of supernova explosions and massive star winds generated in a (circum-)nuclear starburst, are able to compress and sweep the ambient interstellar medium of spiral galaxies with velocities of a few hundred kilometers per second along the direction of the maximum pressure gradient, i.e., in a direction (almost) orthogonal to the disk of the galaxy (Heckman et al. 1990 and references therein). Evidence for such winds has been reported in a number of edge-on spiral galaxies (Veilleux et al. 1994; Lehnert & Heckman 1996; Lehnert, Heckman, & Weaver 1999; Strickland et al. 2002), where the finite thickness of the disk of the galaxy and the central location of the starburst (or AGN) defines the direction of the maximum pressure gradient and therefore of the wind. As already pointed out by McD03, it is, however, very unlikely that the ordered interstellar medium and well-defined geometry of spiral galaxies would exist in advanced mergers such as Arp 220. As shown in the previous sections, the large-scale gas/dust and stellar distribution do show in Arp 220 a complex structure characterized by a central dust lane, a low surface brightness stellar envelope, and broad tidal tails at distances of several kiloparsecs. In addition, the large-scale two-dimensional velocity field does not show any regular pattern with a privileged orientation or spin axis. All these characteristics support the idea that even if a galactic wind is generated in the central region (i.e., inner kiloparsec) as a consequence of a (circum-)nuclear starburst, changes in the velocity structure and physical conditions of the interstellar medium in which the wind expands will disrupt it in an efficient way. With all these caveats in mind, the consistency of the starburst-driven wind scenario with the observed morphology and measured energetics of the plumes is evaluated in the following paragraphs.

Previous high spatial resolution integral field spectroscopy of the nuclear region did detect the presence of three different kinematical components, consistent with rotating gas in a circumnuclear disk plus a tilted, outflowing gas (ACC01). The SE and NW plumes are oriented roughly along the same direction as the outflowing circumnuclear gas and have an orientation similar to that of the spin axis of the circumnuclear rotating gas, suggesting that the plumes of ionized gas could be due to a galactic wind generated by the nuclear starburst. However, the plumes detected in Arp 220 show properties very different from those of the wind-generated structures detected in edge-on spiral galaxies with central starbursts or AGNs (see Table 2 for a summary of the different properties). The morphology of the ionized gas outside the plane of the galaxy in these nearby edge-on spiral galaxies indicates that the gas is concentrated in filaments (NGC 3079), sheets/filaments (M82), hollow shells (NGC 253), or biconical surfaces (NGC 2992). These structures indicate that the gas being ionized is mostly located in the surface of a bubble-like or conelike structure, some with wide opening angles ($\geq 90^\circ$), as in M82, NGC 2992, or NGC 3079, and others with a more focused beam ($\sim 25^\circ$), as in NGC 253. The Arp 220 plumes show, on the contrary, a centrally concentrated optical and X-ray (McD03), emission with, at the present resolution of about 1 kpc, no evidence of being resolved. This puts an upper limit of about 15°–20° for the opening angle if a conelike or bubble-like structure, as detected in nearby spiral galaxies, is assumed. Therefore, if the plumes in Arp 220 were a consequence of a starburst-driven wind, the outflow channel would have to be very narrow, even narrower than the structure detected in NGC 253. Under the wind scenario, a narrow plume indicates a well-collimated outflow. In order to produce this structure, the wind would have to have a lateral expansion velocity much smaller than the outflowing

TABLE 2

EXTENDED IONIZED GAS: ARP 220 VERSUS GALACTIC WINDS IN SPIRAL GALAXIES

Galaxy	Distance[a] (Mpc)	$\log L_{IR}$[b] ($L_\odot$)	$L_{H\alpha}/L_{IR}$[c] (10^{-5})	L_X/L_{IR}[d] (10^{-5})	Extent[e] (kpc)	$M_{H\alpha}$[f] ($10^4\ M_\odot$)	V_{max}[g] (km s^{-1})	Structure[h]	θ[i] (deg)	References
Arp 220 plumes	77.6	12.16	0.14	0.6	7	34	110	Jet	15–20	1, 2
Arp 220 lobes	77.6	12.16	0.16	0.3	24	27	160	Hollow shell	70	1, 2
M82	3.0	10.52	16	2.5	2.4	66	300	Filaments	90	3, 4
NGC 253	3.0	10.46	0.37	1.5	1.3	1	<100	Hollow shell	20–26	3, 4, 5
NGC 2992	31	10.46	274	...	5.6	10^3	200	Biconical	125–135	6
NGC 3079	16	10.49	2.7	6.2	3	10	2000	Filaments	90	3, 4, 7

[a] Distances as given in Heckman et al. 1990 for M82, NGC 253, and NGC 3079 and in Veilleux, Shopbell, & Miller 2001 for NGC 2992.

[b] Luminosities as given in Heckman et al. 1990 for M82, NGC 253, and NGC 3079 and in Veilleux et al. 2001 for NGC 2992.

[c] Hα luminosities corrected for internal reddening, except for Arp 220, for which the observed values given in Table 1 are used.

[d] L_X indicates the soft X-ray luminosity of the extended, diffuse halo X-ray structure as given in McD03 for Arp 220 and Strickland et al. 2004 for M82, NGC 253, and NGC 3079 and scaled to the distances assumed in the second column.

[e] End-to-end size of the bubble- or cone-shaped structure, not corrected for projection effects.

[f] Mass of the ionized gas, assuming an average density of 100 cm^{-3}.

[g] Line-of-sight velocities given (in absolute values) relative to the velocity of the system.

[h] Structure defined from ground-based Hα imaging and/or high-resolution X-ray imaging.

[i] Opening angle of the structures as given in the references, or derived from the published images (M82).

REFERENCES.—(1) This work; (2) McD03; (3) Heckman et al. 1990; (4) Strickland et al. 2004; (5) Strickland et al. 2000; (6) Veilleux et al. 2001; (7) Veilleux et al. 1994.

velocity, and the axis of the maximum pressure gradient would have to be very stable over distances of at least few kiloparsecs. Integral field spectroscopy with higher spatial resolution (0.″5) is needed in order to be able to resolve the plumes and investigate the velocity field across the plume.

Under the galactic wind scenario, the shocks generated by the expanding wind produce an Hα luminosity that is directly proportional to the preshock ambient density and to the total surface of the hollow cone or bubble and has a strong dependence ($\propto V_s^{2.4}$) on the velocity of the shock (see, for instance, Veilleux et al. 2001). Moreover, the total kinetic energy liberated by the starburst-driven wind is a few percent of the energy liberated by supernova explosions and massive stars winds and therefore is directly proportional to the star formation rate (SFR in units of $M_\odot$ yr^{-1}), as given by the expression $E_k = 9.4 \times 10^{54}$SFR ergs, if continuous star formation over a period of 20 Myr is assumed (Colina, Lípari, & Macchetto 1991). According to this, since Arp 220 is a ULIRG, about 50 times more luminous than the nearby spiral galaxies where wind-related structures are detected, the total mass and kinetic energy of the ionized gas in the plumes is expected to be 50 times that measured in spiral galaxies. However, this is not the case. The observed maximum velocity (not corrected for projection effects) is relatively low for large, kiloparsec-scale galactic winds, and the ionized gas mass is in the range measured in nearby galaxies (see Table 2). Moreover, if normalized by the infrared luminosity, the plumes in Arp 220 (and even the plumes with the additional contribution from the lobes) are underluminous in X-ray and Hα emission by factors of at least 10 with respect to galaxies with prototype large-scale, wind-induced structures, including M82, NGC 2992, and NGC 3079 (see Table 2; see also Table 9 in Strickland et al. 2004). Only the small (overall extent of 1.3 kpc) shell detected in NGC 253 has an Hα-to-infrared luminosity ratio similar to those measured in the plumes and lobes of Arp 220.

In summary, the Arp 220's plumes, as traced by the optical emission lines and X-ray emission, are underluminous when compared with the galactic wind structures in nearby spiral galaxies. Therefore, if the starburst-driven wind scenario holds for Arp 220 plumes, the derived energetics indicates that the starburst-driven wind is much less efficient, by factors of at least 10, than that in spiral galaxies with well-developed wind-induced structures. Whether or not this behavior is due to the existence in ULIRGs of an ambient, dense, interstellar medium with a complex three-dimensional structure and a velocity field characterized by not having a privileged kinematical axis, requires further investigations and detailed modeling.

4.2. *Origin of the Lobes: Tidally Induced Structures?*

Although the starburst-driven wind interpretation could still hold as an explanation for the origin of the ionized gas detected in the circumnuclear regions (ACC01) and even in the plumes, the large-scale, i.e., several-kiloparsec–sized, two-dimensional kinematical structure presented here (see § 3.4) does not support this scenario as the origin of the edge-brightened lobes detected in X-rays and Hα. As mentioned in § 3.4, the steepest gradients in the velocity field of the diffuse, extended gas are associated with substructures identified in the stellar light distribution, in particular with the southwestern side of the central dust lane, the eastern extended stellar envelope, and the broad western tidal tail. Therefore, the three-dimensional gas and stellar structure of a merger galaxy, such as Arp 220, makes it difficult to assume a stable axis for the direction of the maximum pressure gradient that, as in edge-on spiral galaxies, would channel the gas from the central regions into the outer envelopes of the galaxy at distances of 10 kpc or larger.

In the following, we explore the scenario of the lobes as a merger by-product in Arp 220. As already pointed out by McD03, the different surface brightnesses and orientations of the plumes and lobes suggest that these two regions are dynamically distinct and point to different origins. Within the framework of the merger scenario, the morphology of the X-ray/Hα lobes, with their edge-brightened structure and orientation, is best fitted by the off-center, face-on collision of two corotating disks with an impact velocity of less than a couple of hundred kilometers per second (McD03). According to the specific dynamical simulation of the Arp 220 merger (see McD03 for detailed explanations), the plumes and lobes are density condensations produced about 150 Myr after closest approach and 15 Myr after the formation of the dense central region. Following this model further, the edge-brightened Hα lobes are expanding outward while also experiencing a general rotation, a remnant of the original rotation of the two disks. The combination of the radial expanding flow and residual rotation of the disks is such that the line-of-sight velocity along each of the lobe rims ranges from +185 to +25 km s^{-1} (E lobe) and from -175 to -20 km s^{-1} (W lobe) in the frame of the galaxy (McD03). The data do not have a high enough signal-to-noise ratio (S/N) to measure accurate velocities for each position along each of the rims, but they are good enough to measure an average velocity for both E and W lobes. The measured velocities, corresponding to $+8 \pm 79$ km s^{-1} for the E lobe and -79 ± 58 km s^{-1} for the W lobe, are to first order in agreement with the predictions, but a more detailed comparison with the models is needed. Since the lobes traced by the optical emission lines have a low surface brightness, low spatial resolution integral field spectroscopy with 10 m class telescopes is required in order to obtain a significant improvement in the quality of the present spectra.

5. SUMMARY

The complex two-dimensional structure, ionization state, and velocity field of the warm ionized gas in the ULIRG Arp 220 has been investigated for the first time over a region of about 75.″0 × 40.″0 (i.e., 28 × 15 kpc), using deep integral field optical spectroscopy with the INTEGRAL system. Arp 220 is the nearest ULIRG, and therefore the complexity of its extended structure, reaching the low surface brightness levels of the ionized gas lobes previously detected in this unique target, has been investigated with unprecedented detail. The main results from this study are

1. The structure of the ionized gas presents three distinct regions at different linear scales that show, as already known, an overall morphology similar to that of the X-ray–emitting gas. The three different regions are (*a*) the circumnuclear region up to a radius of about 5.″0 (2 kpc), already studied in ACC01; (*b*) the elongated, high surface brightness plume at radii between 5.″0 and 10.″0 (2–4 kpc); and (*c*) the extended, low surface brightness lobes at radii between 10.″0 and 35.″0 (4–15 kpc).

2. If the high surface brightness plumes are the result of a starburst-driven galactic wind, the measured energetics traced by the Hα and X-ray luminosities indicates that it must be at least 1 order of magnitude less efficient than the bubble-like or conelike galactic wind structures detected in nearby edge-on galaxies.

Also, the opening angle of the plume in Arp 220 is very narrow ($\sim 20^\circ$) when compared with the wide opening angles typical of wind-generated structures. These nonstandard properties could be caused by the complex three-dimensional structure and kinematics of the gas and stellar components in advanced, luminous mergers, such as Arp 220, which are very different from the ordered galactic structure of edge-on spiral galaxies, where a rotation disk with a finite thickness defines the axis of the outflowing wind, i.e., the axis of the maximum pressure gradient. This deserves proper investigations, with detailed modeling and additional two-dimensional spectroscopy.

3. The kinematics of the lobes, with average velocities of $+8 \pm 79$ km s^{-1} and -79 ± 58 km s^{-1} for the E and W lobe, respectively, are to first order in agreement with the predictions of the tidally induced scenario proposed by McD03, by which the gas condensations in the lobes are products of the merger that are animated by a combination of continuing expansion and residual rotation from the original rotation of the two disks involved in the merger. This scenario has to be explored further by measuring the two-dimensional velocity structure of the gas along the rims of the lobes with spectra having better S/Ns. Low spatial resolution integral field spectrographs mounted on 10 m class telescopes would be needed for this purpose.

4. The two-dimensional velocity field shows its largest gradients (50 km s^{-1} kpc^{-1}) and deviations (+280 to -320 km s^{-1}) from the systemic velocity in the low surface brightness ionized gas associated with the dust lane, the southeastern stellar envelope, and the northwestern broad stellar tidal tail, at distances of up to 7.5 kpc from the nucleus. Therefore, the velocity field of the gas at distances of a few to several kiloparsecs from the nucleus and with peak-to-peak deviations of 600 km s^{-1} is associated with well-defined stellar structures induced by the merger; i.e., it is dominated by tidally induced flows and has no connection with a central, starburst-driven galactic wind.

Additional results are

5. The ionized gaseous plume is elongated along P.A. 120° (southeast) to 320° (northwest), with the SE plume brighter than the NW plume by a factor of 4. An asymmetry in the radiation field as seen by the gas in the plumes is the most likely explanation for this difference. Alternative explanations, such as differences in the gas density and/or absorption effects through the plane of the galaxy, are not supported by the present data.

6. The [N II] and Hα emission peaks are separated by about 1 kpc in both sides of the plume. The ionization structure is such that the [N II] emission is closer to the nucleus and the Hα emission peaks at the tip of the plumes. The ionization state is consistent with its being produced by high-velocity shocks expanding in a neutral ambient medium.

7. The change in the ionization state along the plumes, in particular the NW plume, traced by a change in the [N II]/Hα ratio is interpreted as being produced by discontinuities in the velocity field and/or density of the gas at the interface of the main stellar body of the galaxy with the low surface brightness extended envelope.

8. The NW plume has a fainter, secondary component that runs almost parallel to the main component and south of it. The inner part of this secondary plume is also dominated by the [N II] emission, while the outer region emits in Hα. This change in the [N II]/Hα ratio is interpreted, as in result 7, as produced by variations in the velocity field and/or density of the ambient gas.

9. The lobes show the same structure in both [N II] and Hα, with their peak emissions spatially coincident, within the present resolution. However, contrary to the brightness distribution of the gas in the plumes, here the W lobe has a surface brightness higher than the E lobe by a factor of 3, as previously detected in X-rays.

Luis Colina thanks the Instituto de Astrofísica de Canarias and the Space Telescope Science Institute for their hospitality and financial support. We also thank Luis Cuesta for his help using GRAFICOS. Support for this work was provided by CICYT (Comisión Interministerial de Ciencia y Tecnología), through grants PB98-0340-C01, PB98-0340-C02, and AYA2002-01055. Dave Clements acknowledges funding by PPARC. E-mail exchanges and discussions with D. K. Strickland are also acknowledged.

REFERENCES

Arp, H. 1966, ApJS, 14, 1
Arribas, S., & Colina, L. 2003, ApJ, 591, 791
Arribas, S., Colina, L., & Clements, D. 2001, ApJ, 560, 160 (ACC01)
Arribas, S., & Mediavilla, E. 2000, in ASP Conf. Ser. 195, Imaging the Universe in Three Dimensions: Astrophysics with Advanced Multi-Wavelength Imaging Devices, ed. W. van Breugel & J. Bland-Hawthorn (San Francisco: ASP), 295
Arribas, S., Mediavilla, E., García-Lorenzo, B., & del Burgo, C. 1997, ApJ, 490, 227
Arribas, S., et al. 1998, Proc. SPIE, 3355, 821
Baan, W. A., & Haschick, A. D. 1995, ApJ, 454, 745
Bingham, R. G., Gellatly, D. W., Jenkins, C. R., & Worswick, S. P. 1994, Proc. SPIE, 2198, 56
Carico, D. P., Graham, J. R., Matthews, K., Wilson, T. D., Soifer, B. T., Neugebauer, G., & Sanders, D. B. 1990, ApJ, 349, L39
Clements, D. L., McDowell, J. C., Shaked, S., Baker, A. C., Borne, K., Colina, L., Lamb, S. A., & Mundell, C. 2002, ApJ, 581, 974
Colina, L., Lípari, S., & Macchetto, F. 1991, ApJ, 379, 113
Dopita, M. A., & Sutherland, R. S. 1995, ApJ, 455, 468
Graham, J. R., Carico, D. P., Matthews, K., Neugebauer, G., Soifer, B. T., & Wilson, T. D. 1990, ApJ, 354, L5
Heckman, T. M., Armus, L., & Miley, G. K. 1990, ApJS, 74, 833
Heckman, T. M., Dahlem, M., Eales, S. A., Fabbiano, G., & Weaver, K. 1996, ApJ, 457, 616
Hibbard, J. E., Vacca, W. D., & Yun, M. S. 2000, AJ, 119, 1130
Lehnert, M. D., & Heckman, T. M. 1996, ApJ, 462, 651
Lehnert, M. D., Heckman, T. M., & Weaver, K. A. 1999, ApJ, 523, 575
McDowell, J. C., et al. 2003, ApJ, 591, 154 (McD03)
Sakamoto, K., Scoville, N. Z., Yun, M. S., Crosas, M., Genzel, R., & Tacconi, L. J. 1999, ApJ, 514, 68
Scoville, N. Z., Yun, M. S., & Bryant, P. 1997, ApJ, 484, 702
Scoville, N. Z., et al. 1998, ApJ, 492, L107
———. 2000, AJ, 119, 991
Soifer, B. T., et al. 2000, AJ, 119, 509
Strickland, D. K., Heckman, T. M., Colbert, E. J. M., Hoopes, C. G., & Weaver, K. A. 2004, ApJS, in press
Strickland, D. K., Heckman, T. M., Weaver, K. A., & Dahlem, M. 2000, AJ, 120, 2965
Strickland, D. K., Heckman, T. M., Weaver, K. A., Hoopes, C. G., & Dahlem, M. 2002, ApJ, 568, 689
Surace, J. A., Sanders, D. B., & Evans, A. S. 2000, ApJ, 529, 170
Veilleux, S., Cecil, G., Bland-Hawthorn, J., Tully, R. B., Filippenko, A. V., & Sargent, W. L. W. 1994, ApJ, 433, 48
Veilleux, S., Shopbell, P. L., & Miller, S. T. 2001, AJ, 121, 198